Applied Surface Science 506 (2020) 144756

Contents lists available at ScienceDirect

Applied Surface Science

journal homepage: www.elsevier.com/locate/apsusc

Full Length Article

Free-standing and supported phosphorene nanoflakes: Shape- and size-dependent properties

M.Y. Bakir[a], H.D. Ozaydin[a], T. Gorkan[a], O. Üzengi Aktürk[b], G. Gökoğlu[c], E. Aktürk[a,d,*], S. Ciraci[e]

[a] Department of Physics, Adnan Menderes University, 09100 Aydın, Turkey
[b] Department of Electrical & Electronics Engineering, Adnan Menderes University, Aydın 09010, Turkey
[c] Department of Mechatronics Engineering, Faculty of Engineering, Karabuk University, 78050 Karabuk, Turkey
[d] Nanotechnology Application and Research Center, Adnan Menderes University, 09100 Aydın, Turkey
[e] Department of Physics, Bilkent University, Ankara 06800, Turkey

ARTICLE INFO

Keywords:
Black phosphorene
Blue phosphorene
Nano flakes
Surface interaction
Density functional theory

ABSTRACT

The ultra-small sized nanomaterials are important for basic functional components of future nanoelectronics, spintronics and sensor devices. In this study, based on first-principles density functional theory, the free-standing and supported nanoflakes of bare and hydrogen saturated black and blue phosphorene of diverse size and shape have been investigated. Cohesion, formation energy, thermal stability and electronic structure of these nanoflakes have been revealed. For nanoflakes supported by specific substrates, such as phosphorene, graphene and Mos_2 monolayer, the equilibrium configuration and the binding energy of the flakes, as well as the effects of substrate on the electronic structure have been investigated. While the cohesive and formation energies and HOMO-LUMO gaps of nanoflakes with their edges passivated by hydrogen display clear size, shape and edge geometry dependencies, they are rather dispersed in bare nanoflakes. The binding of phosphorene nanoflakes to two-dimensional (2D) phosphorene, graphene and MoS_2 monolayers is generally weak and originate from van der Waals interaction. Accordingly, when supported by these monolayers, the electronic structure of free-standing nanoflakes can be preserved for critical applications.

1. Introduction

Strictly 2D monolayers of diverse elements and compounds have been brought into focus after the synthesis of graphene [1]. These are monolayers of group-IV elements [2–5], group III-V and group II-VI compounds [2,6–12], and transition metal dichalcogenides [13–20]. More recently, the synthesis of ultrathin, 2D black phosphorus from its layered bulk counterparts, has brought the free-standing 2D monolayers and multilayers of group-VA elements (pnictogens) into focus [21,22]. Later, Liu et al. [23] have revealed the 2D counterpart of black phosphorus, called phosphorene, as a p-type semiconducting material in which phosphorus atoms are sp^3-like hybridized forming a puckered structure like silicene and germanene. Additionally, theoretical studies have predicted free-standing monolayers of group-VA elements, such as nitrogene [24], blue phosphorene having buckled honeycomb structure [25], arsenene [26–28], antimonene [29,30], bismuthene [31,32]. It was shown that these systems are thermally and dynamically stable and suitable for applications at room temperature and above. 2D monolayers and few-layer of black phosphorus, i.e. black phosphorene in symmetric washboard structure (sw-P or α-P) has been successfully isolated by mechanical exfoliation method from black phosphorus which is the most stable three-dimensional (3D) layered form of phosphorus with a weak van der Waals interlayer interactions like graphite [33,34]. Recently, a phosphorene sheet on Au(111) substrate has been synthesized by molecular beam epitaxy technique and the grown structure identified as a blue phosphorene (also named as β-P) sheet [35,36]. The thermal stability and flexibility of α- and β-P have also been studied theoretically;[37] it is suggested that the α-phase is slightly more stable than the β-phase. Nonetheless, since the energy barrier between β- and α-phase is small, the transformation of one phase to the other can be realized without difficulty [37]. Later, various studies unveiled anisotropic thermal, mechanical, and electronic properties of α-P and its nanoribbons [38–41].

The structural, electronic and optical properties of 2D black phosphorene and its applications have been investigated in recent review articles comprehensively [42–44]. The effects of defects and doping on electronic properties of phosphorene together with possible phosphorene-based devices have been reviewed by Carvalho et al. [42].

* Corresponding author.
E-mail addresses: ethem.akturk@adu.edu.tr (E. Aktürk), ciraci@fen.bilkent.edu.tr (S. Ciraci).

https://doi.org/10.1016/j.apsusc.2019.144756
Received 10 May 2019; Received in revised form 29 September 2019; Accepted 16 November 2019
Available online 03 December 2019
0169-4332/

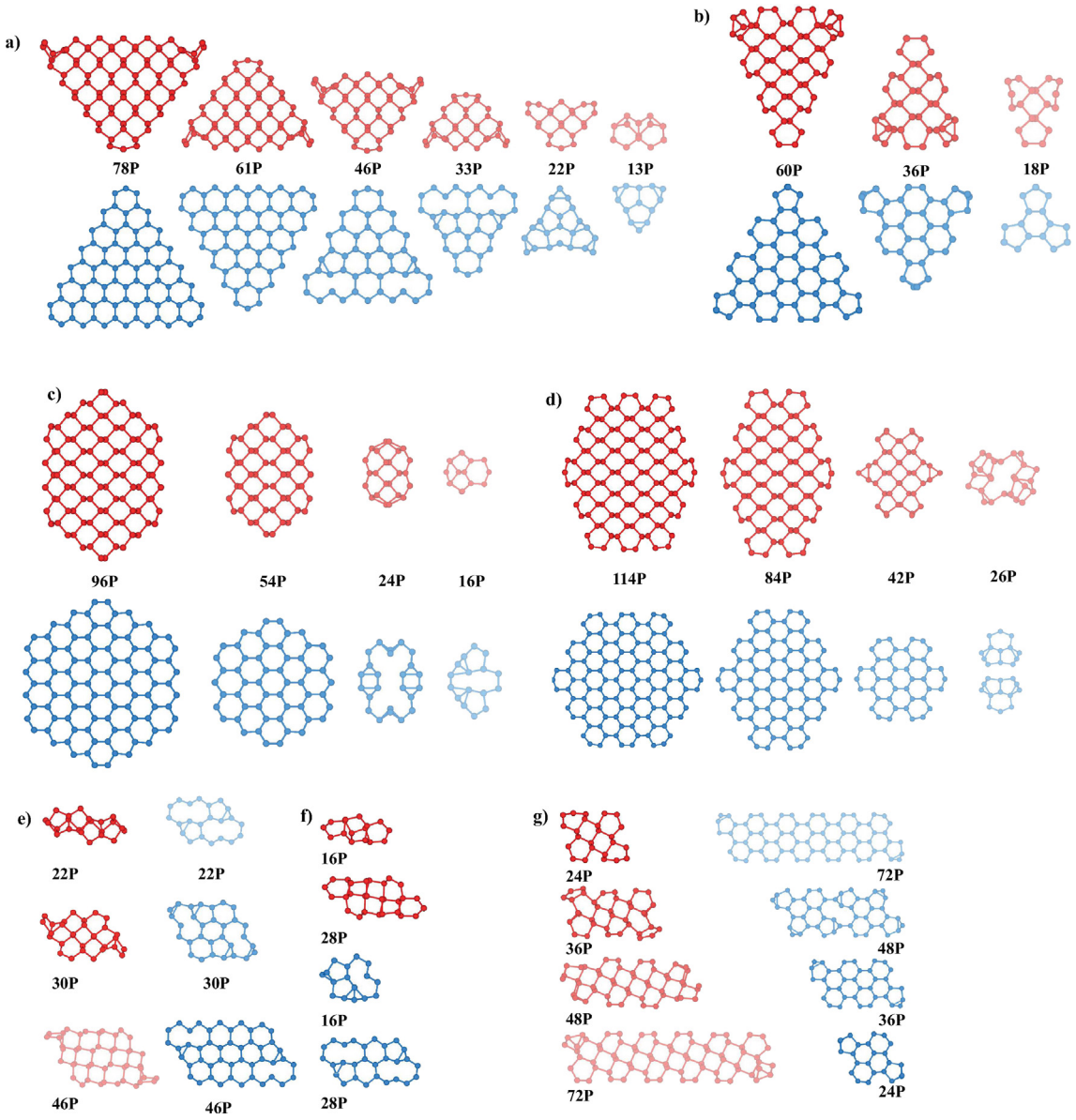

Fig. 1. Atomic structures of bare phosphorene nanoflakes considered in this study. Red: α-PNF and Blue: β-PNF. (a) Triangular-zigzag (t-zz); (b) triangular-armchair (t-ac); (c) coronene-zigzag (c-zz); (d) coronene-armchair (c-ac); (e)-(f) 2-atom and 3-atom based parallelogram-zigzag (p-zz); (g) parallelogram-armchair (p-ac). (For interpretation of the references to colour in this figure legend, the reader is referred to the web version of this article.)

Phosphorene and its structural derivatives, like nanoribbons, nanotubes, fullerenes, and heterostructures have also been reviewed by Sorkin et al. [43], who draw a perspective for opportunities and experimental challenges in phosphorene studies. The properties, fabrication and applications of phosphorene have been discussed by Kou et al. [44], who described the latest developments of more sophisticated design concepts and implementation schemes by addressing some of the challenges in phosphorene research. Additional background related with phosphorene can be acquired from these review articles [42–44].

While 2D monolayers have been treated within the periodic boundary conditions, their finite sheets are actually relevant for various applications. For example, a nanoflake of a 2D monolayer situated on another extended 2D monolayer can be considered as the simplest heterostructure. Nanoflakes can also behave as nanomechanical devices on the surfaces. The nanometer-size flakes of 2D materials on 2D sheets, like graphene flake on graphene [45,46] display crucial dynamical behaviors. It was shown that the translational and rotational displacements of the flakes on graphene surface can generate restoring forces which can lead to a harmonic motion with a characteristic frequency. Due to weak interaction between nanoflake and a 2D monolayer or very thin substrate, low energy barriers involved in the rotational and translational dynamics of nanoflakes keep promises of nearly frictionless motion [47–49]. Consequently, the nanoflakes of 2D monolayers, in particular those of phosphorene have gained importance recently.

In fact, nanoflakes of α-P and β-P, which are essential for diverse nanoelectronic application, display critical geometry and quantum size effects [50,51]. Earlier, the electronic and dielectric properties of only six specific blue phosphorene nanoflakes (β-PNF) have been studied and the possible usage in optoelectronic device applications has been discussed [52]. Zhou et al. [53] studied 12 parallelogram and rectangular nanoflakes of α- and β-PNF. Heterojunctions of nanoflakes of black phosphorene (α-PNF) have been proposed for solar cell applications, since phosphorene has superior properties compared to graphene and MoS_2. [54] α-P has also thickness dependent direct gap ranging between 0.3 eV (bulk) and 1.5 eV (monolayer). Hu et al. [54] report that electronic structure of α-PNFs depends on edge passivation by

Table 1
Optimized values of bare (unpassivated) phosphorene nanoflakes of different types calculated by using PBE: Type of β-PNF; formation energy E_f (meV per P atom); cohesive energy E_c (eV/per P atom); HOMO-LUMO gap E_{H-L} (eV); type of α-PNF; formation energy E_f (meV per P atom); cohesive energy E_c (eV/per P atom); HOMO-LUMO gap E_{H-L} (eV). Here t-ac/18P, as an example, indicates an armchair edged and bare triangular flake comprising 18 P.

	β-PNF			α-PNF		
Type	E_f	E_c	E_{H-L}	E_f	E_c	E_{H-L}
t-ac/18P	185	−3.38	2.13	319	−3.20	0.72
t-ac/36P	145	−3.31	0.38	227	−3.38	0.44
t-ac/60P	174	−3.39	0.92	202	−3.40	0.48
t-zz/13P	373	−3.20	0.65	310	−3.30	0.30
t-zz/22P	310	−3.26	0.12	343	−3.20	0.25
t-zz/33P	276	−3.22	0.11	271	−3.34	0.11
t-zz/46P	254	−3.26	0.07	260	−3.35	0.25
t-zz/61P	236	−3.22	0.81	244	−3.36	0.11
t-zz/78P	219	−3.26	0.56	228	−3.38	0.11
c-ac/26P	350	−3.22	0.62	242	−3.35	0.93
c-ac/42P	236	−3.13	2.23	260	−3.37	0.23
c-ac/84P	312	−3.26	1.86	192	−3.39	1.01
c-ac/114P	265	−3.30	1.85	165	−3.42	1.00
c-zz/16P	371	−3.20	0.43	373	−3.23	1.39
c-zz/24P	302	−3.27	0.55	327	−3.25	0.50
c-zz/54P	303	−3.23	0.10	257	−3.32	0.23
c-zz/96P	154	−3.32	1.62	223	−3.38	0.42
p-ac/24P	341	−3.23	1.89	326	−3.28	0.03
p-ac/36P	213	−3.15	2.09	292	−3.31	0.86
p-ac/48P	304	−3.26	2.03	232	−3.37	0.74
p-ac/72P	379	−3.19	1.86	249	−3.38	0.74
p-zz/16P	409	−3.19	1.10	252	−3.11	0.78
p-zz/22P	478	−3.09	1.35	289	−3.32	0.67
p-zz/28P	290	−3.14	1.04	338	−3.26	0.99
p-zz/30P	333	−3.23	1.02	262	−3.34	0.18
p-zz/46P	212	−3.27	0.77	250	−3.36	0.48

hydrogene and fluorine. Since devices of phosphorene nanoflakes can be fabricated on substrates, substrate-nanoflake interaction is essential. In a theoretical study, Gao et al. [55] investigated the role of substrate, such as Cu(111) and h-BN, on the stabilization of α-PNF nanoflakes. No extensive substrate-phosphorene nanoflake interactions and their effects on the electronic structure are available yet.

In this study, we consider 52 nanoflake systems of black and blue phosphorene of diverse geometry (i.e. triangular (t), coronene (c), and parallelogram (p)) and size with bare and hydrogen passivated zigzag and armchair edges and reveal their structural parameters, cohesion and electronic structures. In this respect, most of the nanoflake systems are studied in this paper for the first time. Since the nanoflakes have to be supported by selected substrates in various applications, the nanoflake-substrate interaction is crucial for whether the initial configuration and electronic properties of the free-standing nanoflake will be maintained on the substrate. Important conclusions of our study are summarized as: (i) bare nanoflakes are prone to instability and edge reconstruction; their properties usually do not show well-defined trends. (ii) Bare nanoflakes of phosphorene can attain stability and durability through the saturation of their edges. Their cohesion, formation energy and HOMO-LUMO gaps display well-defined trends with respect to the number of their phosphorus atoms or size, and their geometrical shape or type. The energy gap decreases with n_P, and approaches to the band gap of their parent 2D monolayers. Nanoflakes with zigzag edges saturated with hydrogen have consistently higher cohesion than its corresponding armchair counterparts. Coronene geometry appears to be most favorable energetically for a given number of P atoms and edge geometry. (iii) The interaction between nanoflakes and supporting 2D monolayer substrates like graphene, phosphorene and MoS_2 is weak, so that the electronic energy structure of free-standing nanoflakes can be maintained when supported.

2. Computational methodology

Calculations are performed within the framework of spin-polarized density functional theory (DFT) using plane-wave basis sets and projector augmented wave (PAW) [56] potentials as implemented in the Vienna ab initio simulation package (VASP)[57]. The exchange correlation potential is approximated with generalized gradient approximation (GGA) using Perdew-Burke-Ernzerhof (PBE) [58] parametrization including van der Waals (vdW) correction. The kinetic energy cut-off for the plane-wave expansion is set to 450 eV. The **k**-point mesh of $1 \times 1 \times 1$ and $3 \times 3 \times 1$ are used for flakes and flake + substrate systems, respectively. Tests for the convergence of the total energy with respect to the **k**-mesh and cut-off energy are carried out. We employ following supercells for substrate + flake systems: The 12×12 supercell for graphene, 9×6 for α-P, 10×10 for β-P, 7×7 for MoS_2. Extensive tests of the energy convergence with respect to the **k**-point mesh and energy cut-off values to be used in the calculations have been carried out. The electronic and geometric relaxation of the structures are performed using rhombic flakes (supercell geometry) with a vacuum distance about 15 Å in all directions, which is large enough to avoid interactions between two adjacent flakes in the periodic arrangement of the supercell method. Atomic positions are optimized using the conjugate gradient (CG) method, where all the atomic coordinates are fully relaxed until the Hellman-Feynman force on each atom is less than 0.001 eV/Å. The energy convergence criteria of the electronic self-consistency was taken as 10^{-5} eV between two successive iterations. Gaussian type Fermi-level smearing method is used with a smearing width 0.01 eV. In order to indicate the stability of PNFs, we have calculated the average cohesive and formation energies. The average cohesive energy (per atom) of a nanoflake, which is edge-passivated by H is calculated as:

$$E_c = (E_{PNFH} - n_P E_P - n_H E_H)/(n_P + n_H) \quad (1)$$

where E_{PNFH} is the calculated total energy of a given edge-passivated nanoflake saturated by H atoms, E_P is the calculated total energy of an isolated P atom, and E_H is that of the isolated hydrogen atom, n_P and n_H are the total number of P and H atoms of the nanoflake, respectively. For the nanoflakes with bare edge (unsaturated) $n_H = 0$. $E_c < 0$ indicates that the formation of a nanoflake is favorable relative to free constituent atoms. Hence, the lower E_c the stronger is the cohesion. The average formation energy (per atom) is calculated as:

$$E_f = (E_{PNFH} - n_P(E_{SL}/n) - n_H(E_{H_2}/2))/(n_P + n_H) \quad (2)$$

n_P and n_H are number of P and H atoms in nanoflake, respectively. E_{PNFH} is the total energy of edge passivated nanoflake, E_{SL} is the total ground state energy of 2D monolayer sheet, n is the number of P atoms in the unit cell of monolayer, and E_{H_2} is the energy of H_2 molecule. For the nanoflakes with bare edge (unpassivated) $n_H = 0$. According to this definition, $E_f > 0$ indicates that formation of a flake from the parent 2D phosphorene phases (and H_2 molecule, if the edges are saturated by H atoms) is not favored energetically. Then, a stable nanoflake with $E_f > 0$ corresponds to local minimum on the Born-Oppenheimer surface. The binding energy and of a specific, edge-passivated nanoflake placed on a monolayer substrate is calculated as:

$$E_b = E_{Sub+PNFH} - E_{PNFH} - E_{Sub} \quad (3)$$

where $E_{Sub+PNFH}$ and E_{Sub} are the total energies of substrate + hydrogen saturated nanoflake and bare substrate, respectively. $E_b < 0$ indicates that there is an attractive interaction between the substrate and the nanoflake providing the binding interaction between them.

We performed charge density analysis and calculated atomic charges by using Bader analysis which presents a good approximation to total charge of an atom [59]. By subtracting the free atom charges from the Bader charges we obtained the charge transfer to the edge passivating hydrogen atoms.

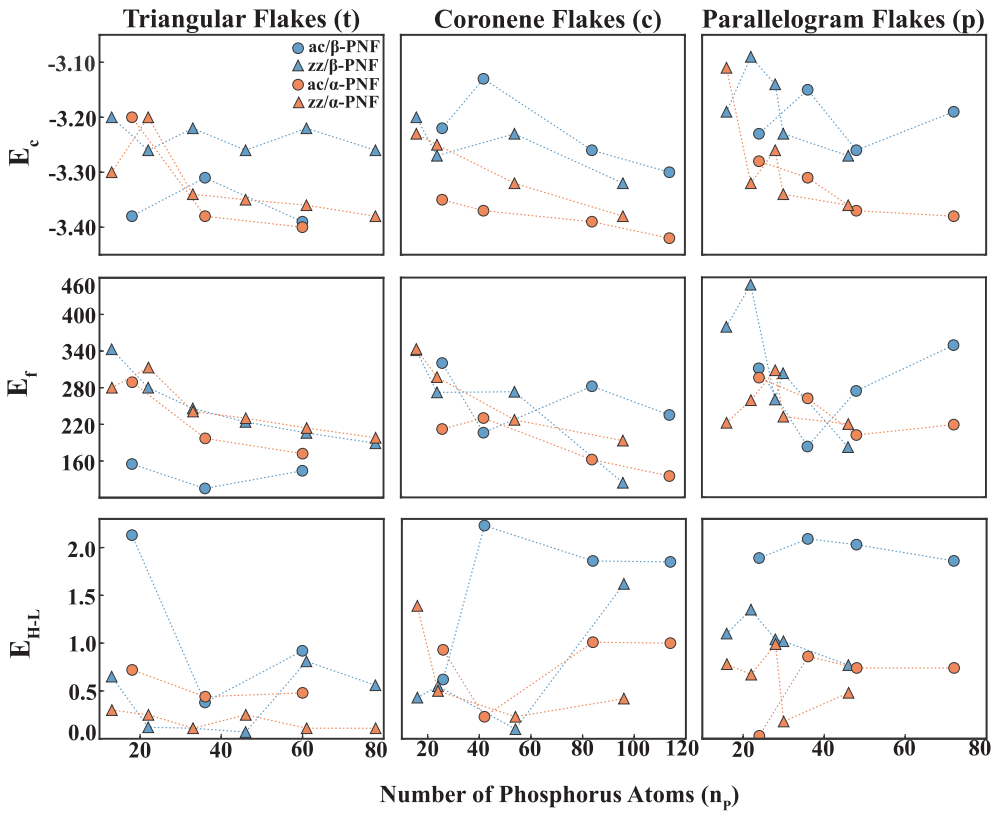

Fig. 2. Variation of the cohesive energy E_c (eV per P atom), the formation energy, E_f (meV per P atom), and HOMO-LUMO energy gap E_{H-L} (eV), with number of P atoms, n_P for bare α-PNF and β-PNF with zigzag (zz) and armchair (ac) edge geometries. From left to right: bare triangular (t), bare coronene (c), and bare parallelogram (p), nanoflakes.

3. Results and discussion

We first calculate the optimized structure, cohesive energy and the fundamental band gap of 2D α-P and β-P monolayers for the sake of comparison with the flakes. The optimized structure of α-P and β-P have cohesive energy, E_c = -3.49 eV and −3.45 eV, respectively. Earlier, Guo et al. [60] calculated these cohesive energies as −3.30 eV/atom and −3.29 eV/atom, respectively. Minute differences between present values and those of Guo et al. [60] are due to different pseudopotentials used in the present and previous calculations. Both α-P and β-P monolayers are semiconductors with fundamental band gap of E_g = 0.88 eV (direct) and 1.88 eV (indirect), respectively. Our results related with the fundamental band gap are in good agreement with previously calculated data [23,25,61].

We now consider a series of bare and hydrogenated α-PNFs and β-PNFs for two commonly known edge structures, i.e. zigzag (zz) and armchair (ac), to investigate the structural stability and electronic properties. We consider three different shapes for nanoflakes; these are triangular(t), coronene(c), and parallelogram (p) structures with zz and ac edge geometries. Edge passivation is usually required for the mechanical and chemical stabilization of a nanoflake. Different kind of atoms can be used to passivate the edges of a nanoflake [37]. He re we passivate zz- and ac-edges by hydrogen atom, while other atoms, e.g. fluorine, can also be used for various purposes like decoration and functionalization [54].

3.1. Bare Phosphorene Nanoflakes, PNF

The triangular nanoflakes of α-PNF and β-PNF with zigzag edges are modelled by flakes consisting of 13,22,33,46,61,78 P atoms as seen in Fig. 1 (a), while their armchair counterparts are modelled by 18,36,60 P atoms. Coronene nanoflakes with armchair edge are formed by 16,24,54,96 P atoms and zigzag ones with 26,42,84,114 P atoms. As for parallelogram nanoflakes, zigzag versions are constructed by 16,22,28,30,46 P atoms and armchair variants by 24,36,48,72 P atoms. In Table 1, we list the values of E_c, E_f, E_{H-L} calculated for bare phosphorene nanoflakes, namely β-PNF and α-PNF, in diverse shapes and sizes. Both phases have average P-P bond length ranging between 2.17 Åand 2.34 Å.

In Fig. 2, we illustrate the variation of calculated cohesive energy, formation energy and HOMO-LUMO gap of bare α-PNF and β-PNF with number of P atoms, n_p, to reveal possible trends. As a result of the structural irregularity, variation of E_c, E_f, and E_{H-L} exhibit irregular behavior without a well-defined trend in size-dependency. Here we point out the general trends unveiled from the plots. The cohesion of bare nanoflakes generally increase (i.e. E_c is lowered) with size or with increasing n_P. The formation energy of flakes (per atom) are small but positive, indicating the fact that the formation of a flake from 2D phosphorene is unfavorable. The general trend displayed by Fig. 2 is that the formation energy per atom decreases with increasing n_P; namely the formation of large nanoflakes become less unfavorable. A few cases of parallelogram nanoflakes go beyond this trend due to their shape and relatively lower coordination number of edge atoms.

Nanoflakes with limited number of n_p are finite size systems and have discrete electronic states instead of bands. The level spacing increases with decreasing n_P due to the confinement of electronic wave function. Also an energy gap occurs between HOMO and LUMO. This gap can be wider with decreasing n_P, as a natural consequence of quantum confinement effect. For bare nanoflakes here, E_{H-L} displays practically a random variation with n_P. Depending on the type (t,c,p), edge geometry (zz,ac) and the parent phase (α, β) the energy gap can vary in the range from 0.1 eV to 2.2 eV due to the dangling bonds states of reconstructed atoms.

It was reported that unpassivated atoms of nanoflake systems can

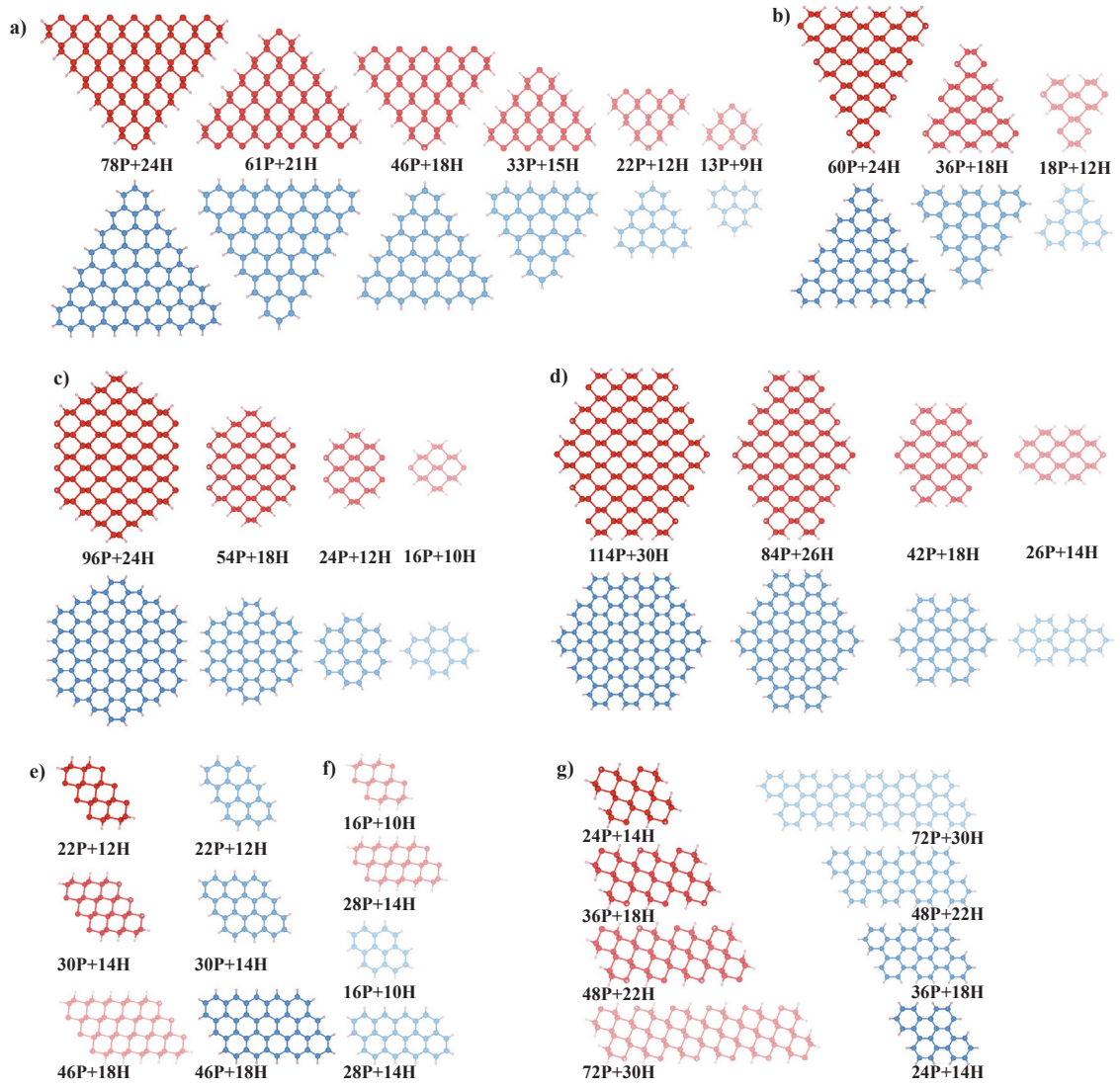

Fig. 3. Atomic structures of edge-passivated, phosphorene nanoflakes considered in this study. Red: α-PNFH and Blue: β-PNFH. (a) Triangular-zigzag (t-zz); (b) triangular-armchair (t-ac); (c) coronene-zigzag (c-zz); (d) coronene-armchair (c-ac); (e)-(f) 2-atom and 3-atom based parallelogram-zigzag (p-zz); (g) parallelogram-armchair (p-ac). (For interpretation of the references to colour in this figure legend, the reader is referred to the web version of this article.)

lead to edge reconstruction, whereby the 2D nature of flakes can be destroyed as shown earlier in graphene flakes [62]. Earlier, edge reconstruction and stability of black phosphorene nanoribbons have been investigated both theoretically and experimentally. [63–66] Edge reconstruction is an exothermic process, where the energy of a nanoflake is lowered and hence the structure reconstructs to attain a structure, which is more stable energetically relative to the ideal structure. Thus, the structural configuration in bare nanoflakes cannot be preserved properly upon reconstruction. In the next section, we will compare the average cohesive energies of bare-reconstructed and hydrogen passivated nanoflakes. It is clearly seen that an edge reconstruction occurs at both armchair and zigzag regions for α- and β-PNFs. The edge reconstruction is very remarkable in small nanoflakes yielding rather asymmetrical structures, so that shapes of these systems are completely destroyed for all triangular, coronene, and parallelogram geometries. Nonetheless, ideal geometry and shape set before the structural optimization are preserved to a large extent for systems with larger than ≈50 atoms. As an extreme case, β-PNF with coronene shape consisting of 26 P atoms is disassociated into two pieces. In this study, we also note that the corner regions with low coordination number are reconstructed as shown in Fig. 1. Accordingly, bare phosphorene nanoflakes are prone to instability, which are undesirable in diverse applications. Under this circumstances, the edges and corners can be passivated by adatoms for a stable and durable configuration, which eventually becomes resistant to structural and electronic changes.

3.2. Hydrogen Passivated Phosphorene Nanoflakes, PNFH

When phosphorene nanoflakes are obtained using mechanical exfoliation, unpassivated structures are stabilized by hydrogen termination of the edge atoms. This way their ideal like configuration are maintained. The edge induced bond strain can have remarkable effects on the structural and electronic properties of small nanoflake systems. It was reported that different passivation groups, e.g. O, H, OH, can induce different effects on electronic structure [67]. We consider H atom for edge passivation, since H-passivation has little influence on the edge morphology, ideal structure and electronic properties. In Fig. 3, we present the atomic configurations of hydrogen passivated phosphorene nanoflakes, α- and β-PNFH of diverse shape, size and edge-geometry. In Table 2, we present the optimized cohesive and formation energies, as well as the HOMO-LUMO gap of these nanoflakes. The average lengths of P-P and P-H bonds in diverse β-PNFH are rather uniform and are stabilized at the value of $\bar{d}_{P-P} = 2.25–2.26$ and $\bar{d}_{P-H} = 1.44$ Å, respectively. While the average length of P-H bonds marks the same value,

Table 2
Optimized values of hydrogen passivated phosphorene nanoflakes of different types calculated by using PBE: Type of β-PNFH; formation energy, E_f (meV per atom); cohesive energy, E_c (eV/per atom); HOMO-LUMO gap E_{H-L} (eV); type of α-PNFH; formation energy, E_f (meV per atom); cohesive energy, E_c (eV/per atom); HOMO-LUMO gap E_{H-L} (eV). Here t-ac/18P + 12H indicates an armchair edged and H passivated triangular flake comprising 18 P and 12 H atoms.

	β-PNFH			α-PNFH		
Type	E_f	E_c	E_{H-L}	E_f	E_c	E_{H-L}
t-ac/18P + 12H	27	−3.02	2.96	29	−3.04	2.69
t-ac/36P + 18H	21	−3.11	2.60	24	−3.14	2.01
t-ac/60P + 24H	18	−3.18	2.41	20	−3.20	1.76
t-zz/13P + 9H	29	−3.01	3.12	34	−3.02	3.03
t-zz/22P + 12H	25	−3.08	2.77	29	−3.10	2.53
t-zz/33P + 15H	22	−3.14	2.62	26	−3.16	2.20
t-zz/46P + 18H	20	−3.18	2.46	23	−3.21	1.96
t-zz/61P + 21H	18	−3.22	2.37	21	−3.24	1.77
t-zz/78P + 24H	16	−3.25	2.28	19	−3.27	1.64
c-ac/26P + 14H	24	−3.09	2.71	28	−3.11	2.09
c-ac/42P + 18H	19	−3.13	2.22	22	−3.19	2.00
c-ac/84P + 26H	15	−3.25	2.25	17	−3.28	1.66
c-ac/114P + 30H	13	−3.28	2.24	15	−3.31	1.47
c-zz/16P + 10H	28	−3.04	2.96	33	−3.06	2.63
c-zz/24P + 12H	24	−3.11	2.77	28	−3.13	2.48
c-zz/54P + 18H	18	−3.22	2.40	21	−3.25	1.87
c-zz/96P + 24H	14	−3.29	2.24	17	−3.32	1.57
p-ac/24P + 14H	25	−3.06	2.71	27	−3.09	2.70
p-ac/36P + 18H	22	−3.11	2.52	24	−3.14	2.31
p-ac/48P + 22H	20	−3.14	2.45	23	−3.16	2.27
p-ac/72P + 30H	19	−3.19	2.38	22	−3.19	2.24
p-zz/16P + 10H	28	−3.04	2.95	31	−3.06	2.87
p-zz/22P + 12H	26	−3.08	2.72	29	−3.10	2.69
p-zz/28P + 14H	24	−3.13	2.55	28	−3.13	2.26
p-zz/30P + 14H	23	−3.13	2.63	26	−3.15	2.42
p-zz/46P + 18H	20	−3.27	1.96	24	−3.21	1.95

$\bar{d}_{P-H} =$ 1.44Å in α-PNFHs, the average length of P-P bonds is smaller and occurs at $\bar{d}_{P-P} = 2.23$ Å. The average electronic charge transferred from nanoflake to each passivating H atoms is calculated to be $\rho_E \sim -1.34$ e.

In Fig. 4, we present the overall behavior and trends depending on the shape, size and edge geometry of H-passivated nanoflakes, α-PNFH and β-PNFH as revealed from the data in Table 2. First, it is seen that the cohesion in terms of average E_c increases gradually with the number of atoms n_P for all nanoflakes; namely for three types of nanoflakes, for two edge geometries and for both α-PNFH and β-PNFH. In view of the fact that the cohesive energies of 2D α-P and β-P are −3.49 eV and −3.45 eV, respectively, the limiting values of E_c can be estimated as $n_P \rightarrow \infty$. This is an indication that the cohesion may increase with increasing flake size. However, it was reported that the stability of larger nanoflakes are more sensitive to temperature [37], so that flake size should be optimized for a given temperature for use in possible applications. Perhaps, this argument stemmed from the large size oscillation (wiggles) on the surface of flakes.

If we compare the calculated average cohesive energies, E_c of bare and edge-passivated nanoflakes as given in Tables 1 and 2, bare and reconstructed nanoflakes appear to have stronger cohesive energy per atom. The difference in average cohesive energies between bare and edge-passivated flakes decreases with flake size. We note however, that the total cohesive energy of a hydrogen-passivated nanoflake, $E_{T,c} = E_{PNFH} - n_P E_P - n_H E_H$, is lower (more energetic) than that of the bare and reconstructed nanoflake, $E_{T,c} = E_{PNF} - n_P E_P$. For example, α-PNFH (β-PNFH) of type t-zz/33P + 15H has $E_{T,c}$ = -151.735 eV (-150.660 eV). Whereas, bare and reconstructed α-PNF (β-PNF) of the same type t-zz/33P has $E_{T,c}$ = -110.014 eV (-106.192 eV). This confirms that nanoflakes gain higher stability through hydrogen passivation as compared the reconstruction of bare nanoflakes.

Nanoflakes with zigzag edges have consistently higher cohesion than its corresponding armchair counterparts. α-PNFHs with zigzag edges are the flakes with highest cohesion among the similar type of nanoflakes, except one case. Generally, for a given n_P the cohesion is higher in coronene nanoflakes, and cohesive energies are ordered as $E_c[p] > E_c[t] > E_c[c]$. Hence, coronene shape (or type) appears to be most favorable energetically for a given n_p and edge geometry. Notably, the energy difference between α-PNFH and β-PNFH is generally small for any n_P, type and edge geometry, like that of their 2D parent monolayers. Hence, the structural transitions from α-phase to β-phase or vice versa can take place by thermal excitation at elevated temperatures, if the energy barrier between them is not high. On the other hand, all the formation energies are positive which means flake structures cannot spontaneously be formed from a phosphorene sheet and H_2 molecule. Formation energies follow a trend that the formation of a H-passivated nanoflake becomes less unfavorable as n_P increases. Our calculations predict that armchair as well as zigzag edged coronene β-PNFHs become energetically least unfavorable as n_P increases.

Average bond length between P atoms $\bar{d}_{P-P} = 2.26$ Å and 2.23 Å for β-PNFH and α-PNFH, respectively. The average length of P-H bonds, $\bar{d}_{P-H} \approx$ 1.44 Å for almost all nanoflakes. These values are consistent with previous studies, where bond lengths of P-P bonds in black phosphorus were reported as 2.22 and 2.24 Å for two different bonds at two layers [68].

Hydrogen atom is more electronegative than P atom; hence it receives always charge from phosphorene atoms at the edges behaving as an acceptor material. This is consistent with previous studies [54]. The effects of passivation of edge atoms by hydrogen on charge distribution of nanoflakes are different for β- and α-phases. While the calculated average charge density of hydrogen atom, $\bar{\rho} \approx$-1.34 e and distributes rather uniformly among passivating H atoms of the former, it ranges between −1.33 e and −1.72 e in α-PNFH nanoflakes. For example, triangular α-PNFH receives more charge as compared to other nanoflakes and hence they become electrically more polarized. This behavior can single out one specific nanoflake from others under external electric field.

The level spacings, as well energy gaps, E_{H-L}, of nanoflakes decrease with increasing n_p, and eventually the band formation of discrete electronic energy states starts to form as the size of the nanoflakes increases, which is also consistent with the previous study investigating phosphorene nanoflakes with larger dimension [54]. Conversely, the level spacing, as well as E_{H-L} increase with decreasing n_P as a manifestation of the quantum confinement effect. The overall variations of E_{H-L} with n_P or with size in the plots in Fig. 4 comply with the above arguments based on quantum confinement effect. For small size ($n_P \sim$ 15), triangular, α-PNFH and β-PNFH, the calculated values of $E_{H-L} \approx$ 3.1 eV. The larger E_{H-L} values can be attributed to the chemical hardness of the flake corresponding to larger chemical stability. Chemical hardness is also a measure of the rigidity of electron clouds to deformations [69]. However, as n_P increases, this wide energy gap starts to decrease and starts to distinguish β-PNFH from α-PNFH. Notably, the energy gap values of zz and ac edge geometries in each phase coincide. The energy gap of α-PNFH attains values lower than that of the β-PNFH; the difference between them is ~ 0.6 eV for $n_P \sim$ 80, but increases with increasing n_P to attain a value of ~ 1.0 eV as $n_P \rightarrow \infty$. The similar trend is also seen for the coronene type nanoflakes. While the overall behavior of the parallelogram complies with the trends of the triangular and coronene types, their non-uniform geometries and relatively smaller size prevent them to show exactly similar trends. It appears that the bulk like behavior of these flakes can be realized only for $n_P >$ 200. Nonetheless, each flake being passivated or unpassivated and having specific type, size, edge geometry and phase can be considered as a unique molecule with well-defined level spacing, E_{H-L}. However, as their sizes increase, all these nanoflakes tend to be similar to either one of the 2D monolayer phases with their well-defined energy band gap.

Earlier, Bhatia et al. [52] have studied optical and electronic properties of β-PNFHs, and reported 2.77 eV, 2.50 eV, and 2.56 eV E_{H-L}

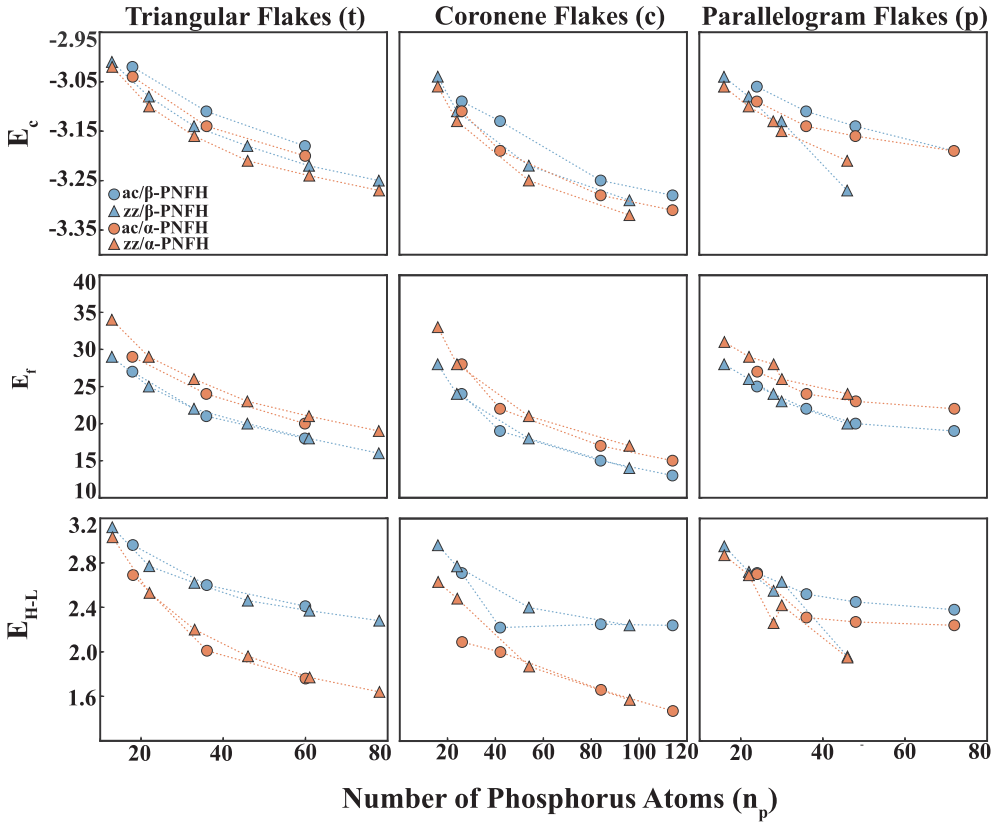

Fig. 4. Variation of optimized values calculated for edge-passivated nanoflakes, α-PNFH and β-PNFH with the number of P atoms, n_P. Cohesive energy, E_c (eV/per atom); formation energy E_f (meV/per atom); HOMO-LUMO band gap E_{H-L} (eV). Nanoflakes have either zigzag (zz) or armchair (ac) edge geometry. From left to right: bare triangular (t), bare coronene (c), and bare parallelogram (p), type nanoflakes.

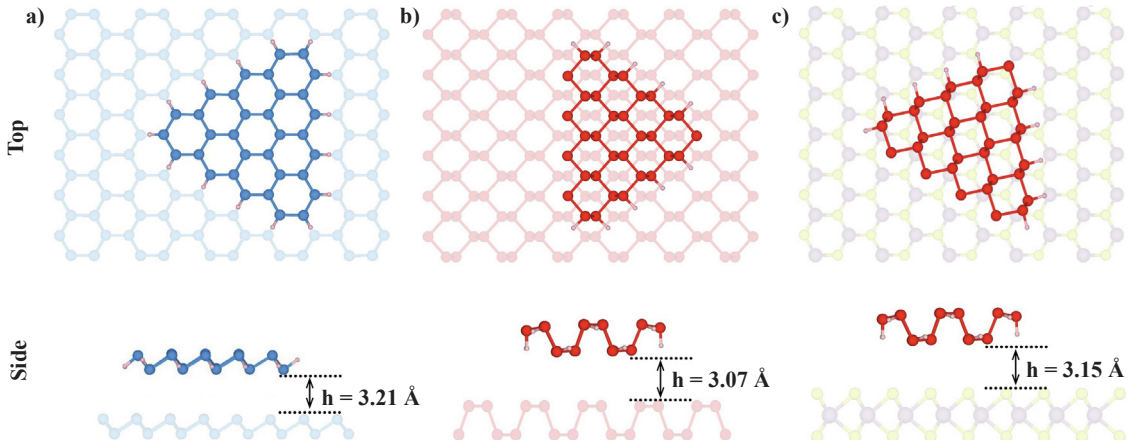

Fig. 5. Top and side views of the atomic configurations corresponding to three different stacking geometry for the supported, triangular phosphorene nanoflakes on different substrate monolayers: (a) AA stacking of a triangular, zigzag edged nanoflake, β-PNFH on 2D blue phosphorene (β-P) monolayer substrate. (b) AB stacking of a triangular, zigzag edged nanoflake, α-PNFH on 2D black phosphorene (α-P) monolayer substrate. (c) AC stacking of a triangular, zigzag edged nanoflake α-PNFH on 2D MoS_2 monolayer substrate. h indicates the minimum spacing between the nanoflake and the monolayers substrate.

values, for hydrogen-passivated t-zz/33P, p-zz/46P, and c-zz/54P. Our corresponding values for similar flakes are 2.62 eV, 1.96 eV, and 2.40 eV. The results are in reasonable agreement. In another work, Hu et al. have studied larger flake systems and they give an approximate gap value as a function of flake length; $E_g = 0.89 + 4.93/L$ for H-passivated flakes. That means for very large flakes E_g converges to 0.89 eV, which is very close to our calculated value of 0.88 eV for α-P sheet [54]. E_{H-L} values of hydrogen passivated black- and blue-phosphorus quantum dots (PQD) with size $n_P = 22 \rightarrow 178$ P atoms have been reported also in a previous study [53]. They report E_{H-L} values 2.52 to 1.36 eV for α-PQDs and 2.85 to 2.14 eV for β-PQDs within the studied range of size. These values are consistent with the present values. Small differences originate from different potentials and methods used in the calculations.

3.3. Supported and hydrogen passivated phosphorene nanoflakes

Since nanoflakes are normally placed on specific substrates to construct heterostructures, nanomechanical device and mediums for superlow frictions, the nature of interaction between the nanoflake and

Table 3
Equilibrium configuration of edge-passivated phosphorene nanoflakes on various monolayer substrates. Type of α-PNFH; monolayer substrate, Subs; equilibrium site; minimum spacing h (Å); the binding energy E_b (eV). Same listing for β-PNFH flakes. Here, t-zz/13P + 9H indicates a zigzag edged and H passivated triangular flake comprising 13 P and 9 H atoms.

	β-PNFH				α-PNFH			
Type	Subs.	Site	h	E_b	Subs.	Site	h	E_b
t-zz/13P + 9H	Grap.	AB	3.20	−1.62	Grap.	AB	3.20	−1.45
t-ac/18P + 12H	Grap.	AA	3.20	−1.96	Grap.	AA	3.12	−1.86
t-zz/22P + 12H	Grap.	AA	3.34	−2.21	Grap.	AA	3.19	−2.02
c-zz/24P + 12H	Grap.	AB	3.27	−2.31	Grap.	AA	3.24	−2.20
p-zz/28P + 14H	Grap.	AA	3.19	−2.58	Grap.	AA	3.31	−2.30
t-zz/33P + 15H	Grap.	AA	3.18	−2.84	Grap.	AA	3.36	−2.57
t-ac/36P + 18H	Grap.	AB	3.39	−3.07	Grap.	AA	3.39	−2.91
t-zz/13P + 9H	β-P	AB	2.97	−1.15	α-P	AB	3.06	−1.09
t-ac/18P + 12H	β-P	AB	3.10	−1.43	α-P	AB	3.02	−1.66
t-zz/22P + 12H	β-P	AB	3.00	−1.80	α-P	AB	2.98	−1.89
c-zz/24P + 12H	β-P	AA	3.10	−1.76	α-P	AB	2.94	−2.14
p-zz/28P + 14H	β-P	AA	3.12	−2.04	α-P	AB	2.99	−2.30
t-zz/33P + 15H	β-P	AA	3.21	−2.43	α-P	AB	3.07	−2.67
t-ac/36P + 18H	β-P	AA	3.17	−2.53	α-P	AB	2.79	−3.12
c-zz/24P + 12H	MoS_2	AA	3.09	−1.97	MoS_2	AC	3.15	−1.72
t-zz/33P + 15H	MoS_2	AA	3.10	−2.69	MoS_2	AC	3.15	−2.14

the substrate becomes crucial. This interaction becomes also critical for the growth of flakes or monolayers on substrates, as well as for the stabilization of nanoflakes. A strong interaction can influence the atomic and electronic structure of nanoflake + substrate system. Under these circumstances the electronic structure of a nanoflake can be also substrate-specific. Strong interaction between substrate atoms and phosphorus atoms of the nanoflakes can lead to destabilization, which results in massive structural reconstruction and clustering. In fact, Gao et al. have theoretically studied the role of substrate on the stabilization of α-PNF nanoflakes [55]. They reported that α-PNF is disassociated on Cu(111) substrate due to strong interaction, while the interaction with h-BN surface is so weak to stabilize α-PNFs. They conclude that a moderate interface interaction is needed to stabilize α-P and also to grow α-P epitaxially. Conversely, a weak interactions, like vdW attraction between nanoflake and substrate is usually desired to attain libration motion with low angular frequencies to construct detectors. Also, weak interaction leads to low energy barriers in rotational and translational dynamics of nanoflakes on substrate, which is essential for nearly frictionless motion. For reason discussed above, the study of the interaction between nanoflake and substrate has been one of our prime objectives.

To unveil the substrate-nanoflake interaction, we investigated specific nanoflakes placed on the selected substrates, namely α-PNFH on graphene, α-P and MoS_2 monolayer substrates; β-PNFHs on graphene, β-P, and MoS_2 monolayer substrates. All the flakes are edge passivated by hydrogen atoms with increased chemical and thermal stability. It was shown that quasi-planar structure of edge passivated free-standing phosphorene nanoflakes are preserved up to 500 K, although flakes have mechanical flexibility [37]. The size of the flakes is varied from 13 P atoms to 36 P atoms (e.g. 13P + 9H, 36P + 18H). The equilibrium configuration corresponding to the minimum (lowest) total energy of a nanoflake + substrate system is obtained by the optimization process explained in computational details, which starts from diverse positions and heights of a nanoflake relative to the selected substrates and minimizes the total energy and atomic forces.

In Fig. 5, we show three typical equilibrium positions of two different flakes on three different substrates. AA, AB, and AC type stacking geometries are considered for flakes on related substrates. Flakes are usually attained the equilibrium height h, of ~3 Åfrom the substrate, which is significantly larger than the P-P bond distance. The wide spacing between the flake and the substrate indicates weak interaction. Equilibrium stacking (or minimum total energy) configuration depends on flake size, since flakes with larger n_p are exposed to larger body forces. Hence, the larger the flake size, the stronger is the binding. All the α-PNFHs are stabilized on α-P substrate in AB-type stacking. However, α-PNFHs on MoS_2 are settled in AC configuration. Same nanoflakes (for $n_p > 13$) are anchored to graphene surface in AA stacking. In Table 3, we present the optimized values, such as the equilibrium stacking, the binding energy E_b, and spacing h, calculated for selected nanoflakes-substrate pairs.

Both α- and β-PNFHs are stabilized on graphene at higher distances compared to their 2D parent sheets. However, the binding energies show different trends. β-PNFHs are adhered to graphene surface more strongly than to β-P and MoS_2 monolayers. As an example, for t-zz/33P + 15H and c-zz/24P + 12H types, the strength of the binding, i.e. the magnitude of E_b, is highest on graphene, but lowest on β-P. The binding is, however, intermediate on MoS_2. As for α-PNFHs, their binding to different substrates displays a size and shape dependent behavior and can deviate from the order given above for β-PNFHs. All the binding energies per phosphorus atom are less than ≈100 meV. This is really a weak binding generated from the weak Van der Waals interaction. Accordingly, we can conclude that, based on these findings, the electronic structures of free-standing nanoflakes presented in Tables 1 and 2 can be preserved even if they are supported by specific substrates in Table 3. Notably, not all substrates couple weakly with phosphorene nanoflakes, but some substrates like Cu(111) interact strongly to dissociate the phosphorene nanoflakes [55].

Since the interactions of the hydrogen passivated phosphorene nanoflakes with the specific substrates are weak and hence the spacings between them are wide, the libration frequency of these flakes on these substrates is expected to be low as predicted earlier for graphene nanoflakes [70]. Moreover, this libration frequency can be affected by a biological molecule, which can be adsorbed to the flake. Hence, the tunable dynamics of the weakly bound phosphorene nanoflakes, which are known to be a biologically important materials, can lead to important biological sensor applications.

4. Conclusions

A large class of phosphorene nanoflakes of diverse type, size and edge geometry with bare and hydrogen passivated edges have been investigated. All nanoflakes considered in this study have cohesion and hence are favorable relative to their free constituent atoms. However, the formations of all nanoflakes are energetically unfavorable relative to the 2D phosphorene phases. The bare (unpassivated) nanoflakes are prone to instability and edge reconstruction. They do not display a well-defined trends with size, due to the edge atoms having small coordination number prone to the reconstruction. Significant amount of electronic charge is transferred from phosphorus atoms to hydrogen atoms when the dangling bonds at the edges are saturated. Consequently the surface of the nanoflake becomes polarized. The flakes, by themselves, attain structural and chemical stability and display well-defined physical properties through passivation by H atoms, and can sustain applications in ambient conditions. Cohesive and formation energies of H-saturated nanoflakes exhibit clear trends depending on their types, sizes, edge geometries and phases. While their cohesion increases with increasing number of phosphorus atoms of the flake, their formation relative to parent 2D phosphorene and H_2 molecule becomes less unfavorable. This means that these nanoflakes (passivated or unpassivated) cannot form spontaneously from the parent 2D phosphorene phases. But they can sustain as a local minimum of the energy once they formed following well-defined kinetic paths. Incidentally, hydrogen passivated nanoflakes in coronene geometry appear to be most favorable energetically for a given number of P atoms and edge geometry. The level spacing and the HOMO-LUMO gap of the

nanoflake depend on whether the dangling bonds at the bare edge are saturated by H atoms. Hydrogen passivated nanoflakes of both black and blue phosphorene display well-defined trends with respect to their size or the number of phosphorus atoms. In particular, the HOMO-LUMO gaps of hydrogen passivated nanoflakes decrease with the increasing size of the flake in compliance with the quantum confinement effects and eventually converge to the band gaps of the 2D phosphorene phases for large number of phosphorus atoms.

Even if the interaction of these nanoflakes with some supporting substrates was shown to be strong and led to its dissociation, we showed that their bindings to specific supporting substrates, like graphene, parent phosphorene and MoS_2 monolayers are weak. Hence, the properties of nanoflakes determined for free-standing state are maintained even when they are supported by these substrates for specific technological applications. Accordingly, each hydrogen passivated nanoflake having a robust atomic and electronic structure can be considered as a unique molecule having specific energy level spacing and HOMO-LUMO energy gap to function as a specific nanodevice or sensor. Therefore, each phosphorene nanoflake offers wide ranges of options for various technological applications. Additionally, their properties can be functionalized and multiplied by doping of magnetic and non-magnetic adatoms, by forming junctions, composite flakes, and insulator-metal-insulator heterostructures for novel devices and sensors.

Declaration of Competing Interest

The authors declare that they have no known competing financial interests or personal relationships that could have appeared to influence the work reported in this paper.

Acknowledgement

Computing resources used in this work were provided by the TUBITAK ULAKBIM, High Performance and Grid Computing Center (TR-Grid e-Infrastructure). This research was supported by the TUBITAK under Project No. 116F059. SC acknowledges the financial support of Academy of Science of Turkey, TÜBA.

Appendix A. Supplementary material

Supplementary data associated with this article can be found, in the online version, at https://doi.org/10.1016/j.apsusc.2019.144756.

References

[1] K.S. Novoselov, A. Geim, S. Morozov, D. Jiang, Y. Zhang, S. Dubonos, I. Grigorieva, A. Firsov, Electric field effect in atomically thin carbon films, Science 306 (2004) 666–669.
[2] E. Durgun, S. Tongay, S. Ciraci, Silicon and III-V compound nanotubes: structural and electronic properties, Phys. Rev. B. 72 (2005) 075420.
[3] S. Cahangirov, M. Topsakal, E. Akturk, H. Sahin, S. Ciraci, Two- and one-dimensional honeycomb structures of silicon and germanium, Phys. Rev. Lett. 102 (2009) 236804.
[4] P. Vogt, P. DePadova, C. Quaresima, J. Avila, E. Frantzeskakis, M.C. Asensio, A. Resta, B. Ealet, G.L. Lay, Silicene: compelling experimental evidence for graphenelike two-dimensional silicon, Phys. Rev. Lett. 108 (2012) 155501.
[5] Y. Xu, B. Yan, H.-J. Zhang, J. Wang, G. Xu, P. Tang, W. Duan, S.-C. Zhang, Large-gap quantum spin hall insulators in tin films, Phys. Rev. Lett. 111 (2013) 136804.
[6] K.S. Novoselov, D. Jiang, F. Schedin, T.J. Booth, V.V. Khotkevich, S.V. Morozov, A.K. Geim, Two-dimensional atomic crystals, Proc. Natl. Acad. Sci. U.S.A. 102 (2005) 10451–10453.
[7] H. Sahin, S. Cahangirov, M. Topsakal, E. Bekaroglu, E. Akturk, R.T. Senger, S. Ciraci, Monolayer honeycomb structures of group-IV elements and III-V binary compounds: first-principles calculations, Phys. Rev. B 80 (2009) 155453.
[8] M. Topsakal, E. Akturk, S. Ciraci, First-principles study of two- and one-dimensional honeycomb structures of boron nitride, Phys. Rev. B 79 (2009) 115442.
[9] E. Bekaroglu, M. Topsakal, S. Cahangirov, S. Ciraci, First-principles study of defects and adatoms in silicon carbide honeycomb structures, Phys. Rev. B 81 (2010) 075433.
[10] M. Topsakal, S. Cahangirov, E. Bekaroglu, S. Ciraci, First-principles study of zinc oxide honeycomb structures, Phys. Rev. B 80 (2009) 235119.
[11] V.O. Ozcelik, E. Durgun, S. Ciraci, New phases of germanene, J. Phys. Chem. Lett. 5 (2014) 2694–2699.
[12] D. Kecik, A. Onen, M. Konuk, E. Gurbuz, F. Ersan, S. Cahangirov, E. Akturk, E. Durgun, S. Ciraci, Fundamentals, progress, and future directions of nitride-based semiconductors and their composites in two-dimensional limit: a first-principles perspective to recent synthesis, Appl. Phys. Rev. 5 (2018) 011105.
[13] K.F. Mak, C. Lee, J. Hone, J. Shan, T.F. Heinz, Atomically thin MoS2: a new direct-gap semiconductor, Phys. Rev. Lett. 105 (2010) 136805.
[14] B. Radisavljevic, A. Radenovic, J. Brivio, V. Giacometti, A. Kis, Single-layer MoS2 transistors, Nat. Nanotechnol. 6 (2011) 147–150.
[15] M. Chhowalla, H.S. Shin, G. Eda, L.L. Li, K.P. Loh, H. Zhang, The chemistry of two-dimensional layered transition metal dichalcogenide nanosheets, Nat. Chem. 5 (2013) 263–275.
[16] L. Rapoport, Yu. Bilik, Y. Feldman, M. Homyonfer, S.R. Cohen, R. Tenne, Hollow nanoparticles of WS2 as potential solid-state lubricants, Nature 387 (1997) 791–793.
[17] C. Ataca, H. Sahin, E. Akturk, S. Ciraci, Mechanical and electronic properties of MoS2 nanoribbons and their defects, J. Phys. Chem. C 115 (2011) 3934–3941.
[18] C. Ataca, M. Topsakal, E. Akturk, S. Ciraci, A comparative study of lattice dynamics of three- and two-dimensional MoS2, J. Phys. Chem. C 115 (2011) 16354–16361.
[19] H.G. Füchtbauer, A.K. Tuxen, P.G. Moses, H. Topsøe, H. Besenbacher, J.V. Lauritsen, Morphology and atomic-scale structure of single-layer WS2 nanoclusters, Phys. Chem. Chem. Phys. 15 (2013) 15971–15980.
[20] M. Javaid, D.W. Drumm, S.P. Russo, Greentree A.D.A study of size-dependent properties of MoS2 monolayer nanoflakes using density-functional theory, Sci. Rep. 7 (2017) 9775.
[21] L. Li, Y. Yu, G.J. Ye, Q. Ge, X. Ou, H. Wu, D. Feng, X.H. Chen, Y. Zhang, Black phosphorus field-effect transistors, Nat. Nanotechnol. 9 (2014) 372–377.
[22] F. Ersan, D. Kecik, V.O. Ozcelik, Y. Kadioglu, O. Akturk Uzengi, E. Durgun, E. Akturk, S. Ciraci, Two-dimensional pnictogens: a review of recent progresses and future research directions, Appl. Phys. Rev. 6 (2019) 021308.
[23] H. Liu, A.T. Neal, Z. Zhu, Z. Luo, X. Xu, D. Tomanek, P.Y. Peide, Phosphorene: an unexplored 2D semiconductor with a high hole mobility, ACS Nano 8 (2014) 4033–4041.
[24] V.O. Ozcelik, O. Akturk Uzengi, E. Durgun, S. Ciraci, Prediction of a two-dimensional crystalline structure of nitrogen atoms, Phys. Rev. B 92 (2015) 125420.
[25] Z. Zhen, D. Tomanek, Semiconducting layered blue phosphorus: a computational study, Phys. Rev. Lett. 112 (2014) 176802.
[26] C. Kamal, M. Ezawa, Arsenene: Two-dimensional buckled and puckered honeycomb arsenic systems, Phys. Rev. B 91 (2015) 085423.
[27] D. Kecik, E. Durgun, S. Ciraci, Stability of single-layer and multilayer arsenene and their mechanical and electronic properties, Phys. Rev. B 94 (2016) 205409.
[28] D. Kecik, E. Durgun, S. Ciraci, Optical properties of single-layer and bilayer arsenene phases, Phys. Rev. B 94 (2016) 205410.
[29] O. Akturk Uzengi, V.O. Ozcelik, S. Ciraci, Single-layer crystalline phases of antimony: antimonenes, Phys. Rev. B 91 (2015) 235446.
[30] Z. Zhang, Z. Yan, Y. Li, Z. Chen, H. Zeng, Atomically thin arsenene and antimonene: semimetal-semiconductor and indirect-direct band-gap transitions, Angew. Chem. Int. Ed. 54 (2015) 3112–3115.
[31] E. Akturk, O. Akturk Uzengi, S. Ciraci, Single and bilayer bismuthene: stability at high temperature and mechanical and electronic properties, Phys. Rev. B. 94 (2016) 014115.
[32] F. Ersan, E. Akturk, S. Ciraci, Stable single-layer structure of group-V elements, Phys. Rev. B 94 (2016) 245417.
[33] Y. Zhang, N. Dong, H. Tao, C. Yan, J. Huang, T. Liu, A.W. Robertson, J. Texter, J. Wang, Z. Sun, Exfoliation of STable 2D black phosphorus for device fabrication, Chem. Mater. 29 (2017) 6445–6456.
[34] A. Castellanos-Gomez, L. Vicarelli, E. Prada, J.O. Island, K.L. Narasimha-Acharya, S.I. Blanter, D.J. Groenendijk, M. Buscema, G.A. Steele, J.V. Alvarez, Isolation and characterization of few-layer black phosphorus, 2D Mater. 1 (2014) 025001.
[35] W. Zhang, H. Enriquez, Y.F. Tong, A. Bendounan, A. Kara, A.P. Seitsonen, A.J. Mayne, G. Dujardin, H. Oughaddou, Epitaxial synthesis of blue phosphorene, Small 14 (2018) 1804066.
[36] J.L. Zhang, S. Zhao, C. Han, Z. Wang, S. Zhong, S. Sun, R. Guo, X. Zhou, C.D. Gu, K.D. Yuan, Z. Li, W. Chen, Epitaxial growth of single layer blue phosphorus: a new phase of two-dimensional phosphorus, Nano Lett. 16 (2016) 4903–4908.
[37] D. Bodi, T. Höltzl, Thermal stability and flexibility of hydrogen terminated phosphorene nanoflakes, J. Phys. Chem. C 122 (2018) 8535–8542.
[38] H. Chen, P. Huang, D. Guo, G. Xie, Anisotropic mechanical properties of black phosphorus nanoribbons, J. Phys. Chem. C 120 (2016) 29491–29497.
[39] Z. Cui, G. Xie, F. He, W. Wang, D. Guo, W. Wang, Atomic-scale friction of black phosphorus: effect of thickness and anisotropic behavior, Adv. Funct. Mater. 4 (2017) 1700998.
[40] H. Gong, P. Zhu, L. Si, X. Zhang, G. Xie, M-shape nanoscale friction anisotropy of phosphorene, Comput. Mater. Sci. 150 (2018) 364–368.
[41] J. Qiao, X. Kong, Z.-X. Hu, F. Yang, W. Ji, High-mobility transport anisotropy and linear dichroism in few-layer black phosphorus, Nat. Commun. 5 (2014) 4475.
[42] A. Carvalho, M. Wang, X. Zhu, A.S. Rodin, H. Su, A.H.C. Neto, Phosphorene: from theory to applications, Nat. Rev. Mater. 1 (2016) 16061.
[43] V. Sorkin, Y. Cai, Z. Ong, G. Zhang, Y.W. Zhang, Recent advances in the study of phosphorene and its nanostructures, Crit. Rev. Solid State 42 (2017) 1–82.
[44] L. Kou, C. Chen, S.C.J. Smith, Phosphorene: fabrication, properties, and applications, Phys. Chem. Lett. 6 (2015) 2794–2805.
[45] F. Peymanirad, S.K. Singh, H. Ghorbanfekr-Kalashami, K.S. Novoselov, F.M. Peeters, M. Neek-Amal, Thermal activated rotation of graphene flake on graphene, 2D Mater. 4 (2017) 025015.
[46] O.U. Akturk, E. Akturk, H.H. Gurel, S. Ciraci, Tunable dynamics of a flake on

graphene: libration frequency, Phys. Rev. B 95 (2017) 125413.
[47] I.V. Lebedeva, A.A. Knizhnik, A.M. Popov, O.V. Ershova, Y.E. Lozovik, B.V. Potapkin, Fast diffusion of a graphene flake on a graphene layer, Phys. Rev. B 82 (2010) 155460.
[48] S. Cahangirov, C. Ataca, M. Topsakal, H. Sahin, S. Ciraci, Frictional figures of merit for single layered nanostructures, Phys. Rev. Lett. 108 (2012) 126103.
[49] S. Cahangirov, S. Ciraci, V.O. Ozcelik, Superlubricity through graphene multilayers between Ni(111) surfaces, Phys. Rev. B 87 (2013) 205428.
[50] J. Tesch, P. Leicht, F. Blumenschein, L. Gragnaniello, A. Bergvall, T. Löfwander, M. Fonin, Impurity scattering and size quantization effects in a single graphene nanoflake, Phys. Rev. B 95 (2017) 075429.
[51] E. Peng, N. Todorova, I. Yarovsky, Effects of size and functionalization on the structure and properties of graphene oxide nanoflakes: an in silico investigation, ACS Omega 3 (2018) 11497–11503.
[52] P. Bhatia, R. Swaroop, A. Kuma, Tunable electronic and dielectric properties of beta-phosphorene nanoflakes for optoelectronic applications, RSC Adv. 6 (2016) 101835–101845.
[53] S. Zhou, N. Liu, J. Zhao, Phosphorus quantum dots as visible-light photocatalyst for water splitting, Comput. Mater. Sci. 130 (2017) 56–63.
[54] W. Hu, L. Lin, C. Yang, J. Dai, J. Yang, Edge-modified phosphorene nanoflake heterojunctions as highly efficient solar cells, Nano Lett. 16 (2016) 1675–1682.
[55] J. Gao, G. Zhang, Y.W. Zhang, The critical role of substrate in stabilizing phosphorene nanoflake: a theoretical exploration, J. Am. Chem. Soc. 138 (2016) 4763–4771.
[56] P.E. Blöchl, Projector augmented-wave method, Phys. Rev. B 50 (1994) 17953.
[57] G. Kresse, J. Furthmuller, Efficient iterative schemes for ab initio total-energy calculations using a plane-wave basis set, Phys. Rev. B 54 (1996) 11169.
[58] J.P. Perdew, K. Burke, M. Ernzerhof, Generalized gradient approximation made simple, Phys. Rev. Lett. 77 (1996) 3865.
[59] W. Tang, E. Sanville, G. Henkelman, A grid-based Bader analysis algorithm without lattice bias, J. Phys.: Condens. Matter 21 (2009) 084204.
[60] H. Guo, N. Lu, J. Dai, X. Wu, X.C. Zeng, Phosphorene nanoribbons, phosphorus nanotubes, and van der Waals multilayers, J. Phys. Chem. C 118 (2014) 14051–14059.
[61] D.A. Ospina, C.A. Duque, J.D. Correa, E.S. Morell, Twisted bilayer blue phosphorene: a direct band gap semiconductor, Superlattices Microstruct. 97 (2016) 562–568.
[62] A.S. Barnard, I.K. Snook, Thermal stability of graphene edge structure and graphene nanoflakes, J. Chem. Phys. 128 (2008) 094707.
[63] P.M. Das, G. Danda, A. Cupo, W.M. Parkin, L. Liang, N. Kharche, X. Ling, S. Huang, M.S. Dresselhaus, V. Meunier, M. Drndićć, Controlled sculpture of black phosphorus nanoribbons, ACS Nano 10 (2016) 5687–5695.
[64] A. Carvalho, A.S. Rodin, A.H. Castro Neto, Phosphorene nanoribbons, EPL 108 (2014) 47005.
[65] L. Liang, J. Wang, W. Lin, B.G. Sumpter, V. Meunier, M. Pan, Electronic bandgap and edge reconstruction in phosphorene materials, Nano Lett. 14 (2014) 6400–6406.
[66] A. Ramasubramaniam, A.R. Muniz, Ab initio studies of thermodynamic and electronic properties of phosphorene nanoribbons, Phys. Rev. B 90 (2014) 085424.
[67] H. Xiao, S. Guo, C. Zhang, C. He, J. Zhong, Effects of edge reconstruction on the common groups terminated zigzag phosphorene nanoribbon, J. Phys. D: Appl. Phys. 50 (2017) 195301.
[68] X. Ling, H. Wang, S. Huang, F. Xia, M.S. Dresselhaus, The renaissance of black phosphorus, Proc. Natl. Acad. Sci. 112 (2015) 4523–4530.
[69] A. Chutia, F. Cimpoesu, H. Tsuboi, A. Miyamoto, Influence of surface chemistry on the electronic properties of graphene nanoflakes, Chem. Phys. Lett. 503 (2011) 91–96.
[70] O. Uzengi Akturk, E. Akturk, H.H. Gurel, S. Ciraci, Tunable dynamics of a flake on graphene: libration frequency, Phys. Rev. B. 95 (2017) 125413.